In-situ Full Scale Load Tests and Estimation Method of Pile Resistance for Nodular Diaphragm Wall Supporting High-rise Tower

K. Watanabe[1] and T. Sudo[2]
[1]*Geotechnical Engineering Department, Technical Research Institute, Obayashi Corporation, Tokyo, Japan*
[2]*Specialty Construction Department, Obayashi Corporation, Tokyo, Japan*
[1]*E-mail*: watanabe.koji.ro@obayashi.co.jp
[2]*E-mail*: watakoji1128@gmail.com

ABSTRACT: In recent years, the height and weight of buildings have increased; a trend noticeable especially in the central urban areas of Japan. Additionally, overturning moments from earthquakes and wind loads cause tensile and compressive forces to occur in pile and wall foundations. These situations result in the development of new types of foundations for high-rise superstructures. The nodular diaphragm wall is one type of such foundation; the nodular part is located at the middle depth. The study presented here was to evaluate the applicability of the nodular diaphragm wall for high-rise towers. A review of foundations similar to the nodular diaphragm wall was first made, followed by an outline description of the high-rise tower. The tension and compression load tests performed on the foundation elements are then presented, and finally a discussion of the design formula for the nodular diaphragm wall.

KEYWORDS: Nodular diaphragm wall, High-rise tower, In-situ full-scale load test, Tension resistance, Compression resistance

1. INTRODUCTION

The Construction of a 634 m highrise tower operational in December 2012 started in July 2008 with the scheduled completion in 2011 . It mainly functions as an antenna tower for broadcasting in the Tokyo metropolitan area. The design of the foundation of the tower was carried out for large earthquake and wind type of loads. In the preliminary design stage two alternatives for the foundation were considered. They are the counter weight plan open caisson (see Figures 1(a) and 2); and nodular SRC (Steel Reinforced Concrete) diaphragm wall (Figure 1(b)). The latter foundation is a newly developed foundation type that has nodular parts in the middle section of the wall. Finally, the nodular type foundation was adopted. It was thought that the former foundation type (open caisson sunk by self-weight0, was dragging the surrounding ground excessively. In contrast, the latter foundation type has minor influence on neighboring existing structures; additionally, can reduce the construction cost and time compared to the former foundation type. The size of the nodular diaphragm is 20 m width, 1.2 m thick and 45 m depth. Appropriate estimation of the tensile resistance as well as the bearing capacity of the diaphragm wall against large earthquakes and/or large wind loads was a main concern in the foundation design. Therefore, tensile and compression load tests on the diaphragm wall was planned. However, load tests on the full-size diaphragm wall were practically difficult. Hence, load tests were carried out on a test nodular diaphragm (4 m width, 1.2 m thick and 45 m depth, see Figure 2,) at the construction site of the high-rise tower in order to obtain design parameters for the full-size diaphragm wall.

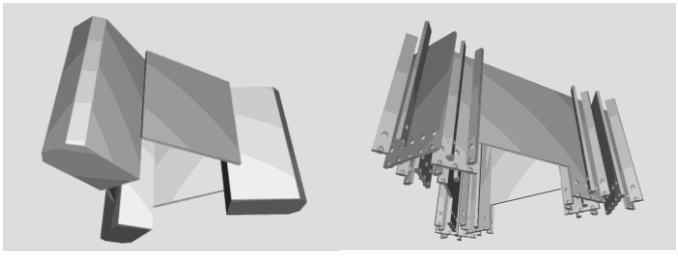

(a) Open caisson plan (b) Nodular diaphragm wall

Figure 1 Alternative of foundation types

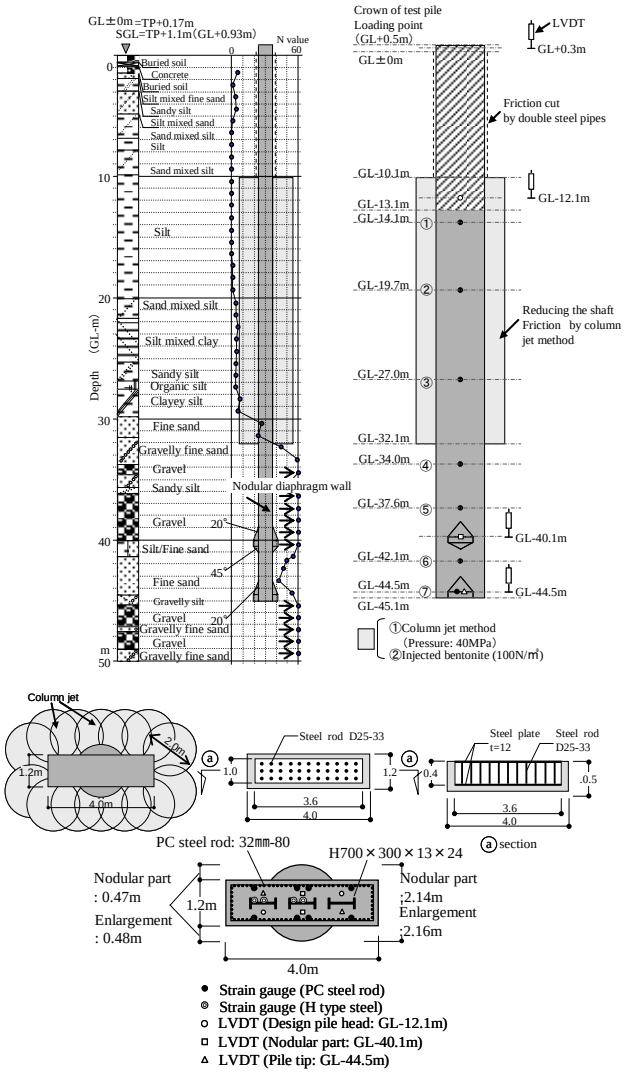

Figure 2 Soil profile and test diaphragm wall

This paper firstly reviews foundations similar to the nodular diaphragm wall, secondly describes the outline of the high-rise tower including design loads, then presents the tension and compression load tests, and finally discusses the design formula for the nodular diaphragm wall.

2. OUTLINE OF THE SUPERSTRUCTURE AND DESIGN LOADS

2.1 Outline of the high-rise tower

An outline of the high-rise tower is reported by Keii et al. (2009). Figure 3 indicates the site plan for the area of the high-rise tower. The construction site is located in between Kita-Jukken river and Tobu Railway. The site plan is divided into three areas that involve commercial area, tower area and office area. The high-rise tower is located in the center of the site.

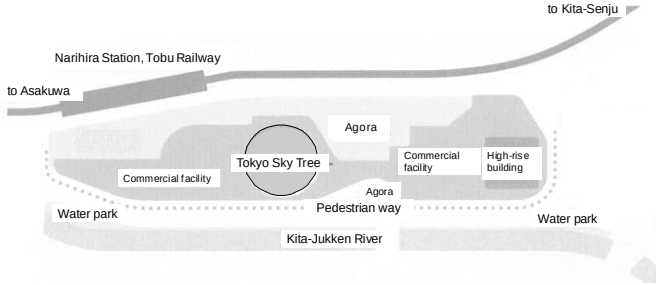

Figure 3 Site plan for the area of the high-rise tower

A schematic view of the high-rise tower is shown in Figure 4. The high-rise tower reached its maximum height of 634 m. The high-rise tower has two observatories at 350 m and 450 m; and the upper part higher than 500 m functions as a for broadcasting tower. The shape of the sectional area changes as the height of tower increased. The lower part of tower has triangular shape, while the higher part has circular shape.

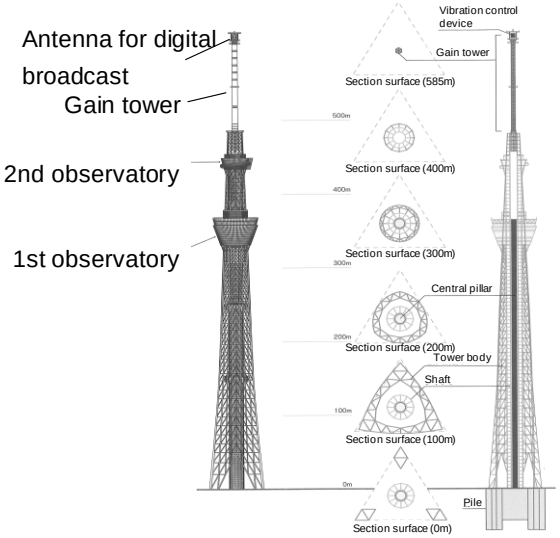

Figure 4 Schematic view of high-rise tower

The high-rise tower is supported by a foundation structure consisting of three SRC walls; cast-in-place concrete piles and a number of nodular diaphragm walls (see Figures 5 and 6). The foundation structure has a triangular shape with a width of about 79 m. At each apex of the triangular part, several nodular diaphragm walls having different sizes are constructed. The size of the largest nodular diaphragm wall is 1.2m by 20 m in cross-section; composed of five elements and 45 m in length.

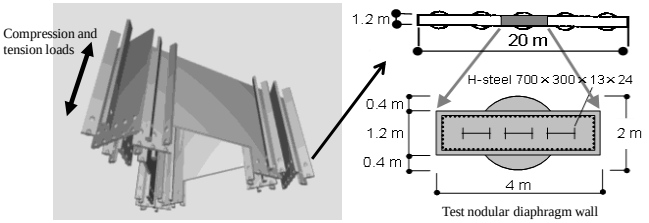

Figure 5 Foundation structure and test diaphragm wall

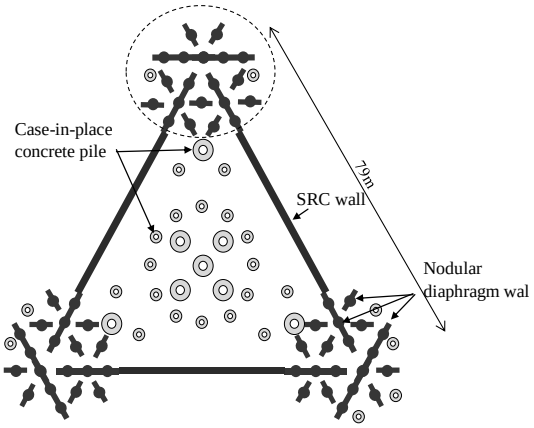

Figure 6 Plan view of foundation

2.2 Design loads

The design loads externally on the high-rise tower are the self-weight storm wind load and earthquake load. Three levels were considered for both storm wind and earthquake as shown in Tables 1 and 2. Note that level 3 earthquake is an expected nearby large earthquake. The self-weight of high-rise tower is about 400 MN.

Table 1 Design storm wind levels and design maximum loads

Level of storm wind	Recurrence period (year)	Wind speed (m/s)
Level 1	100	36
Level 2	500	40
Level 3	2000	43

Table 2 Design earthquake levels and design maximum loads

Level of earthquake	Recurrence period (year)	Magnitude
Level 1	475 (rare)	Past maximum strong motion
Level 2	970 (very rare)	M7.0 to 8.6
Level 3		Expected nearby epicentral earthquake (M6.9)

Table 3 indicates the required performance of the high-rise tower. The high-rise tower was designed so that stresses in structural members remain in elastic region against the combination of storm winds and earthquakes of level 2.

The design of the foundation was carried out against the combination of storm wind and earthquake of level 3. The maximum over-turning moment on the tower was estimated by conducting seismic response analysis of the tower structure alone using the expected ground surface acceleration as input acceleration at the bottom of the tower, disregarding the foundation structure. The overturning moment by the wind loads was also considered.

Table 3 Required performance of the high-rise tower against various load levels

Level of loads	Recurrence period (year)	Required performance
Level 1 Wind Level 1 Earthquake	100 475	No damage
Level 2 Wind Level 2 Earthquake	500 970	Nearly no damage (structural members remain elastic)
Level 3 Wind Level 3 Earthquake	2000	Not collapse

From the estimated over-turning moment, the maximum tension load at diaphragm wall group at each apex of the triangular foundation was estimated as 240 MN with consideration of the self-weight of the tower. In this estimation, compression and tension resistances of the SRC (steel reinforced concrete) walls and the cast-in-place concrete piles were neglected for a safe design. As a safety factor of 3 was employed, the required ultimate tension capacity of each diaphragm wall group was 720 MN.

Much care was not taken for the compression resistance of the diaphragm wall group, because the diaphragm walls were embedded in very hard layers having SPT N-values much larger than 60 by 12 m depth.

3. LOAD TEST DESCRIPTION

As mentioned in the previous section, the required ultimate tension capacity of each diaphragm wall group was 720 MN. As it was really difficult to confirm the tension capacity of the diaphragm wall group by conducting a tension load test, tension load tests on an element of the diaphragm wall (see Figure 5) were carried out. The test nodular diaphragm wall was one element that had a cross-section of 1.2m by -4.0 m was performed. The test wall had nodular parts and pile base enlargements as shown in Figure 2 and Photo 1.

Photo 1 Test nodular diaphragm wall having nodular parts and pile base enlargements

The diaphragm wall group consists of 20 diaphragm elements although widths of the diaphragm walls in the group are different. A target value of the tension capacity of the test diaphragm wall was roughly estimated as 36 MN (720/20 MN). It is noted that when actual diaphragm walls consist of 3 (or 5) pieces of the test diaphragm walls, the ultimate tension capacity of the actual diaphragm wall is expected to be less than 3 times (or 5 times) the ultimate tension capacity of the test diaphragm wall. Hence, it was decided to apply a tension load of 43 MN that is 20% higher than 36 MN.

Reaction beam and reaction pile system was employed to apply loads on the test wall. Table 4 shows the specifications of the test wall and the reaction piles (Figure 7). The profiles of soil layers and SPT N-values at the test site have been shown in Figure 2, together with the seating of the test wall. The nodular parts were located at a depth of around 40 m where silty fine sand having SPT N-value greater 40 existed, while the wall base was sat on the gravel layer below 50 m depth. Friction cut by a double pipe method was carried out from the ground level to a depth of 10 m, because that depth was the design wall head.

Table 4 Specifications of test diaphragm wall and reaction piles

	Pile configuration	Pile length	Depth of pile head	Depth of pile tip	Diameter of nodular part	Diameter of under-reamed part	Maximum load	
							Tensile	Compressive
	(m)	(m)	(m)	(m)	(m)	(m)	(MN)	(MN)
Test wall	1.2 x 4.0	45.0	11.0	45.0	2.00 (2.14)	2.00 (2.16)	40 43*	 40*
Reaction pile	D1.5	50.0	-	50.0	-	-	-	-
* After reducing shaft friction around test pile								
D: Pile diameter								

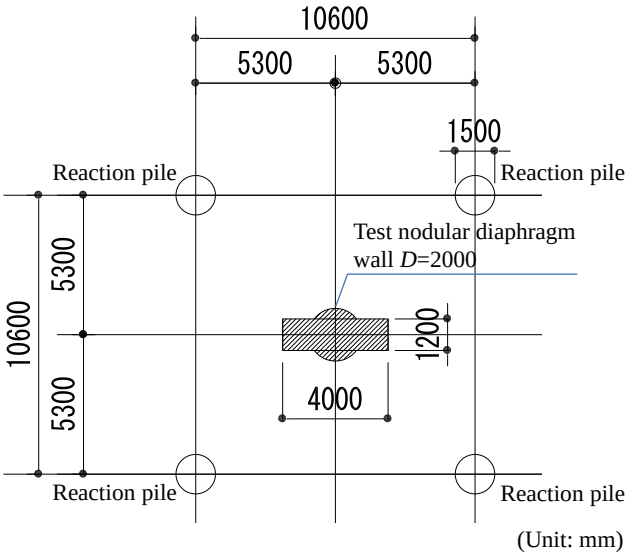

Figure 7 Arrangement of test diaphragm wall and reaction piles

The primary purpose of the load test was to obtain relationship of tension load and tension displacement at the design wall head level. The maximum load capacity in compression and tension of the reaction system used was 48 MN. Three kinds of load tests were planned to be carried out on the same test diaphragm wall to confirm the tension and compression resistances of the nodular parts. The load tests included 1) Tension load test, 2) Tension load test with reducing the shaft friction around the test diaphragm wall, 3) Compression load test with reducing the shaft friction around the test diaphragm wall. That is, after the first tension load test, friction cut by a jet grouting method using bentonite liquid was carried out to a depth of 32 m (see Figure 2) to decrease the shaft friction aiming at increasing load transmitted to the nodular parts.

In addition, the compression resistance of the base of the test wall was reduced by placing an apparatus as shown in Photo 2 beneath the wall base. This apparatus consisted of 33 steel rods sandwiched by two steel plates. The group of steel rods yields when a compression

load of 1.4 MN is applied. Hence, the compression base resistance of the test wall was limited to 1.4 MN in the compression load test.

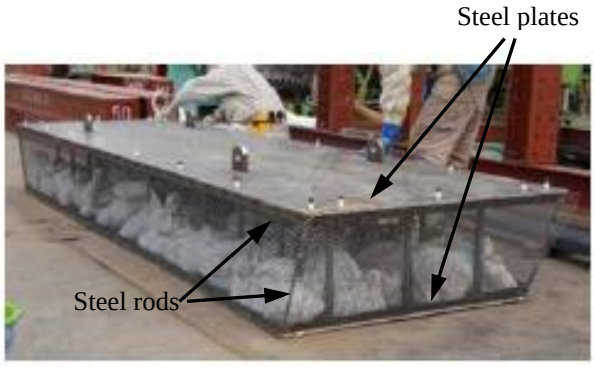

Photo 2 Reduction apparatus of bearing capacity

All the load tests were carried out following JGS (Japanese Geotechnical Society) standard of vertical load test method (2002). Loading method was a multiple cycle method with stepwise loading. Holding time for each loading step was 30 minutes for new loading steps and zero load steps and 2 minutes at repeated loading steps. Displacements at the design wall head (10 m below the ground surface), nodular part and pile tip, the applied load at the wall head, and strains of PC steel rods and H-shaped steels at seven levels of the test wall were measured. The measured strains were used for estimating axial forces in the test wall.

4. RESULTS OF LOAD TESTS

4.1 Tensile load test

In order to estimate tensile axial forces from the measured strains of PC steel rod and H-shaped steels in the test wall, Young's modulus and cross-sectional area of each cross-section indicated in Table 5 were used. In order to take into account non-linear stress-strain behavior of the concrete material, the relationship between tension axial stress, σ, and tension axial strain, ε, shown in Figure 8 was employed. Naganuma and Yamaguchi (1990) reported the softening characteristics of concrete in tension loading. The cyclic behavior of reinforced concrete was summarized by Naganuma and Ohkubo (2000). Based on these works, the relationship between tension stress and tension axial strain of the test diaphragm wall was estimated as shown in Figure 8. The tension stress (or force) of the test wall was estimated from the measured strain using the stress-strain curves in Figure 8. The relation indicated by the solid line was used for new loading steps, while the relations indicated by the dashed lines were used for repeated loading steps.

Table 5 Calculation conditions

	Elastic modulus	Sectional area
	N/mm^2	mm^2
Concrete	See Fig. 8	4.67×10^6
PC steel rod	1.97×10^5	6.43×10^4
H steel (Flange)	2.09×10^5	4.32×10^4
H steel (Web)	2.06×10^5	2.63×10^4

Loading sequence in the first tension load test is shown in Figure 9. The maximum tension load of 42 MN was applied in the 10th loading step. Figure 10 shows the relations of tension load at the loading point and tension (upward) displacements at the loading point, the design wall head, the nodular part and the pile base.

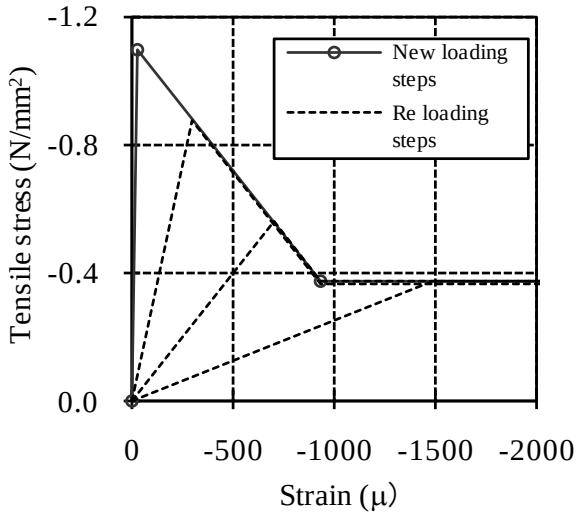

Figure 8 Relationships between tensile stress and strain on concrete

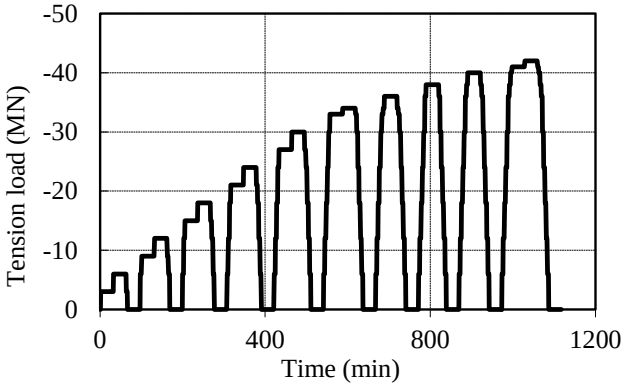

Figure 9 Load cycles

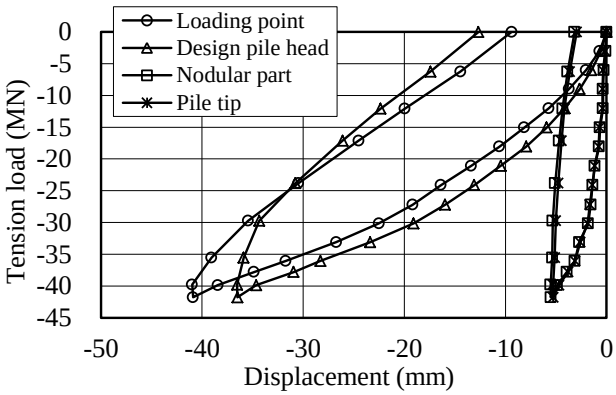

Figure 10 Curves of tensile load at loading point and displacement

Note that tension force and upward displacement are taken as negative (compression force and downward displacement as positive) in this paper. Figure 11 shows the relationship between the tension load and the upward displacement at the design wall head. It is inferred from Figure 11 that the tension load would have increased exceeding -40 MN. However, the load test was terminated due to the limitation of load capacity of the loading system used, as mentioned earlier.

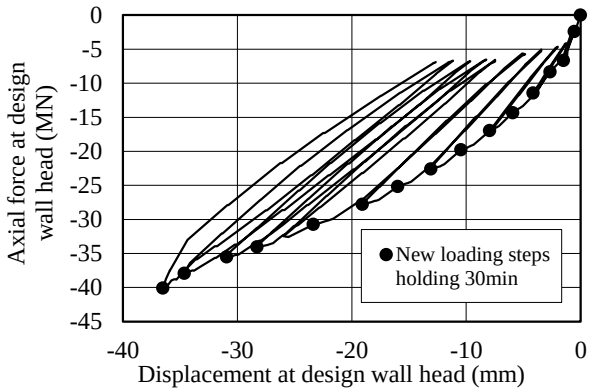

Figure 11 Relationship between axial force and displacement at design wall head

The distributions of axial force and shaft friction are shown in Figure 12. The shaft friction of each wall section was calculated as difference of axial forces divided by the corresponding surface area. Surface area of the nodular part or the under-reamed part was allowed for, if it existed. It can be seen from Figure 12 (a) that the tension loads transferred to the nodular part and the under-reamed part were very small, even when the maximum tension load of 42 MN was applied at the loading point, resulting in small mobilized shaft resistance at these parts as shown in Figure 12 (b). Figure 13 shows the relationship between the shaft friction and the local pile displacement for each wall section. From these figures, the following findings were obtained. The shaft friction to a depth of 34 m was fully mobilized, and the shaft resistance to a depth of 27 m exhibits a nearly elastic-perfect plastic behaviour while the shaft resistance between depths of 27 m to 34 m exhibits a softening behaviour. It is also seen that the shaft resistance below a depth of 34 m did not reach limit values and tended to increase much more if a larger tension load had been applied.

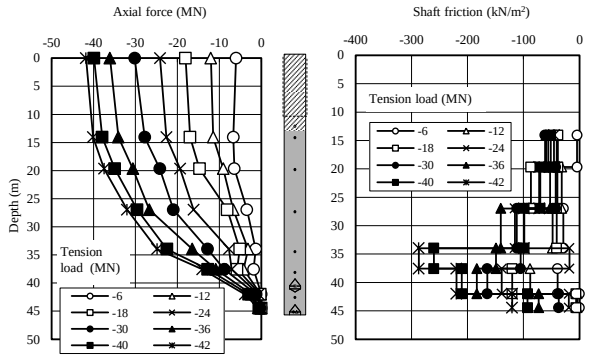

(a) Axial force (b) Shaft friction

Figure 12 Distributions of axial force and shaft friction

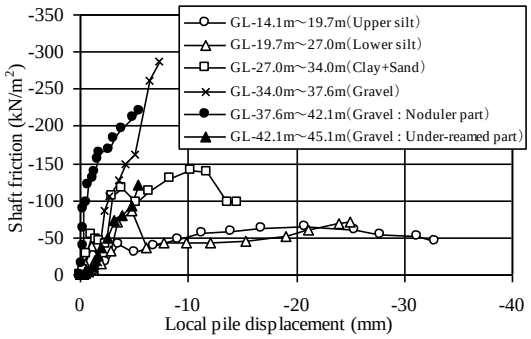

Figure 13 Relationships between shaft friction and local pile displacement

The cross-section of the wall was divided into three blocks (blocks A, B and C) as shown in Figure 14 in order to investigate the distributions of strains in plane at each level of strain measurement. The distributions of strains in planes at level 5 (above the nodular part, GL-37.6 m) and level 6 (below the nodular part, GL-42.1 m) are shown in Figure 14. At level 5, strains at block C are higher than those at blocks A and B when the loads greater than 36 MN were applied. This may indicate that axial force concentrates in block C due to the existence of nodular part. Considering this phenomenon, the axial force of each block was approximately calculated using the strain measured at each block. After that, the bearing forces of both the nodular part and the under-reamed part were calculated from the axial forces of block C at levels 5, 6 and 7. The bearing force was then divided by the projection area of the nodular part or the under-reamed part to estimate the bearing pressure, p_v. Figure 15 shows the relationships between p_v and the local pile displacement for the nodular part and the under-reamed part. The bearing pressures, p_v, of the nodular part and the under-reamed part reached 5800kN/m^2 and 1500kN/m^2 at displacements of 5.5 and 5.3mm, respectively. These bearing pressures did not reach limiting values and tended to increase when the maximum tension load of 42MN was applied. In order to obtain the limiting values of p_v for the nodular part and the under-reamed part, a second tension load test was carried out after the friction cut work to a depth of 32.1 m (see Figure 2).

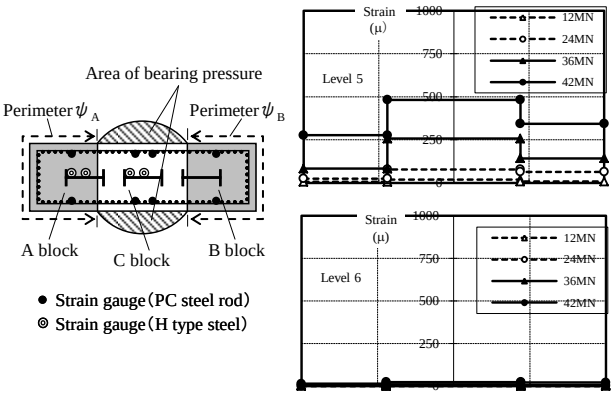

Figure 14 Sectional distributions of strain

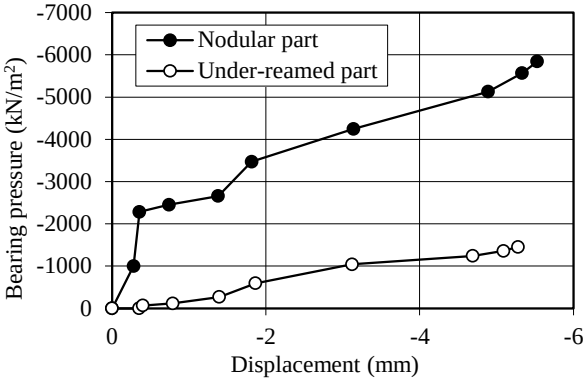

Figure 15 Relationships between bearing pressure and displacement

4.2 Tension load test with reducing the shaft friction around the test wall

Loading sequence in the second tension load test is shown in Figure 16, in which the maximum tension load of 42 MN was applied in the 9th loading cycle. Three loading cycles were carried out (in 6th, 7th and 8th loading cycles) before reaching the maximum load, aiming at reducing the shaft friction around the test wall. The residual strains and displacements after the completion of the friction cut work

were not measured because the measurement transducers were dismounted during the friction cut work. Therefore, strains and displacements of the test wall were set at zero prior to the start of the second tension load test.

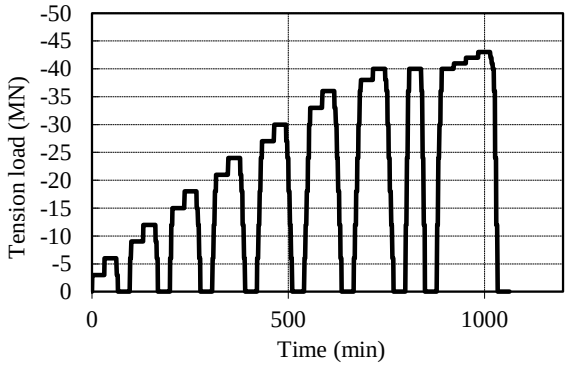

Figure 16 Load cycles

Figure 17 shows the relationships between the tension load at the loading point and displacements at the loading point, the design wall head, the nodular part and the under-reamed part. The yielding behaviors are clearly detected for the nodular part and the under-reamed part.

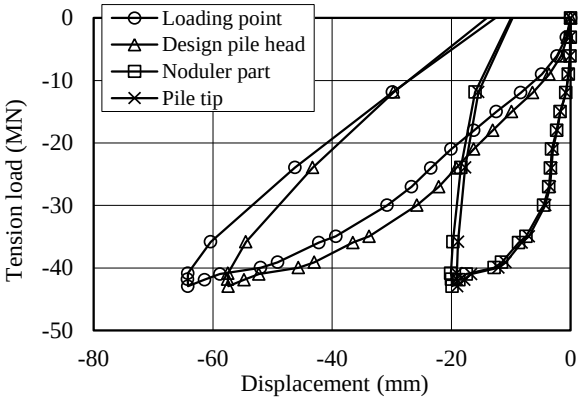

Figure 17 Curves of tensile load at loading point and displacement

As the friction cut was carried out to a depth of 34 m, the relationship between the axial force and the displacement at the depth of 34 m is shown in Figure 18. A clear yielding behaviour can be seen also in this curve.

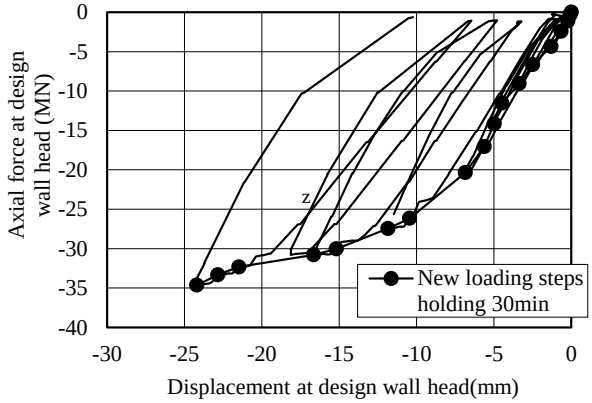

Figure 18 Relationship between axial force and displacement at design wall head

Distributions of axial forces and shaft friction are shown in Figure 19. Although reduction of axial forces is seen between the ground surface and a depth of 14 m, axial forces along the friction cut work section are almost constant with depth (Figure 19 (a)), resulting in almost zero shaft friction along this section (Figure 19 b)). It can be seen from Figure 19 (b) that the shaft friction below a depth of 34 m is higher compared to the first tension test (Figure 12 (b)). Figure 20 shows the relationship between the shaft friction and the local pile displacement for each wall section. Higher shaft friction is mobilized for depths deeper than 34 m, compared to the first tension load test (Figure 13).

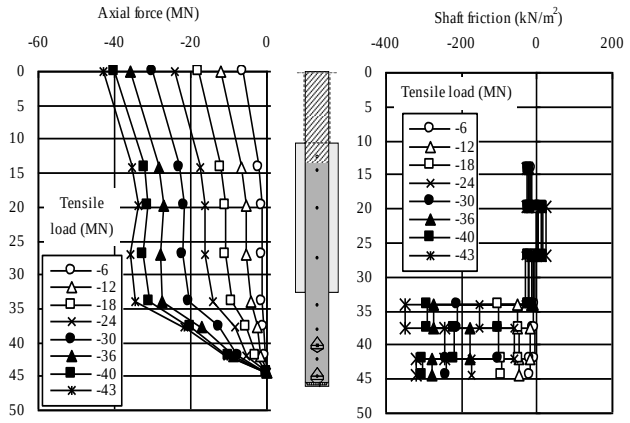

(a) Axial force (b) Shaft friction

Figure 19 Distributions of axial force (left) and shaft friction (right)

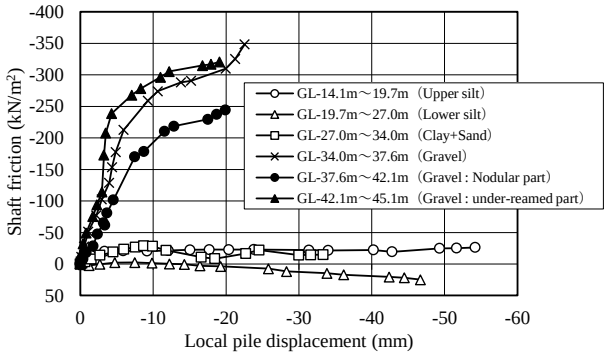

Figure 20 Relationships between shaft friction and displacement

The bearing pressures, p_v, at the nodular part and the under-reamed part were calculated using the same manner as described in section 4.1. The relationships between bearing pressure and displacement are shown in Figure 21. Here, the tension resistance at the pile tip was assumed as zero. Clear yielding behaviour is seen for both the nodular part and the under-reamed part. The bearing pressures at the maximum load of 42 MN are 6450kN/m^2 at a displacement of 29 mm for the nodular part and 3000kN/m^2 at a displacement of 19 mm for the under-reamed part. These values are greater than those in the first tension load test (Figure 15), especially for the under-reamed part. The purpose of tension load tests is to investigate the tension resistance which is larger than 36MN of the design requirement value. It is concluded from the results of tension load tests that the nodular diaphragm wall has the design requirement tension resistance. Thus, the foundation which supports the high-rise tower has been constructed as originally planned.

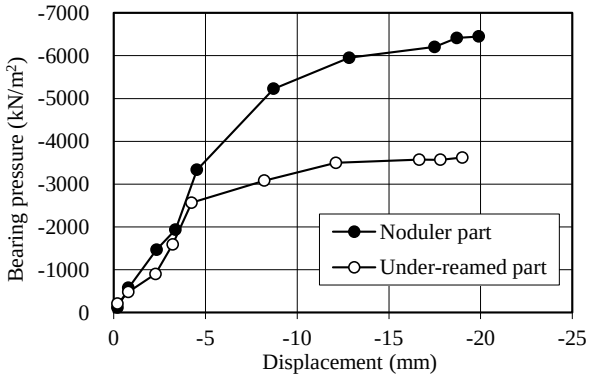

Figure 21 Relationships between bearing pressure and displacement

4.3 Compression load test with reducing the shaft friction around the test wall

Compression load test on the test wall was carried out subsequently to the second tension load test to investigate the behavior of the test wall in compression loading. Residual tension strains in the wall generated in the second tension test turn to compression strains during the compression load test. When measured strain becomes compression, Young's modulus of the concrete was estimated from the relation shown in Figure 22 and the compression axial force was calculated using the Young's modulus corresponding to the measured strain level.

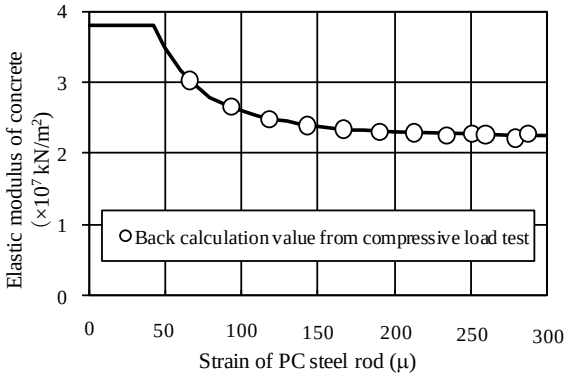

Figure 22 Elastic modulus of concrete

Loading sequence in the compression load test is shown in Figure 23, in which a maximum compression load of 40 MN was reached in the 8th loading cycle. Hereafter, results of the compression load test are presented together with the results of the second tension test for purpose of comparison. It should be noted again that the friction cut work was done to a depth of 34 m.

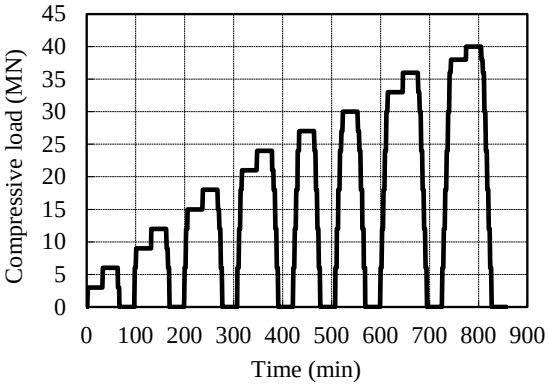

Figure 23 Load cycles

Figure 24 shows the relationship between the load at the loading point and displacements at four different levels of the test wall. It can be seen that load-displacement curves at all the different levels in compression loading are almost linear, whereas the responses in tension loading exhibit highly non-linear behaviors. A possible reason for this may be the generation of tension cracks in the concrete cross-section of the test wall.

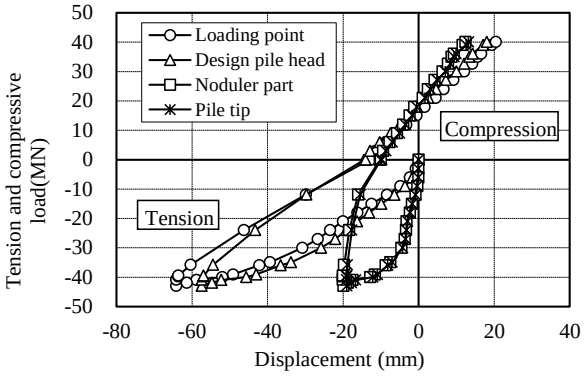

Figure 24 Relationship between load and displacement at the loading point in tension and compression load tests

Relationship between the load and the displacement at the loading point, relationship of axial force and displacement at a depth of 34 m, the distributions of axial force and shaft friction, relationship between shaft friction and local wall displacement in stage of the compression load test and relationship between bearing pressures at the nodular part and the under-reamed part and local wall displacements are shown in Figures 25 to 28. The bearing pressure of the nodular part was calculated using the same method as mentioned in section 4.1. From the results in these figures, the following findings are pointed out.

1) It can be seen from Figure 25 that the stiffness (load increment/ displacement increment) of the load-displacement curves at the design wall head is larger in the compression test than in the tension test. This is attributed to generation of micro tension cracks in the test wall when a tension load greater than 6MN was applied. It is also seen that compression load started to mobilize when the compression displacement of 2 mm occurred after the start of the compression load test. This may be explained by voids between the nodular part and the ground below them which have been generated during the preceding tension load test.

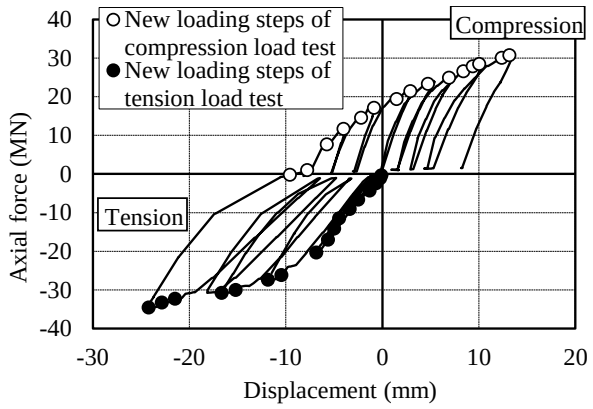

Figure 25 Relationship between axial force and displacement at design wall head

2) It can be seen from Figure 26 that the resistance of the test diaphragm wall in both tension and compression is almost mobilized at the nodular part and the under-reamed part, indicating the large contribution of these parts in the compression and tension resistances of the diaphragm wall. It can be also seen from Figure 27 that the shaft friction at the nodular part was fully mobilized while the shaft resistance at the under-reamed part tended to increase even when the displacement at the loading point reached 13 mm.
3) The bearing pressure at the nodular part as shown in Figure 28 indicates the maximum value of p_v=10,000kN/m^2. It can be concluded that the nodular part has large resistance in compression test.

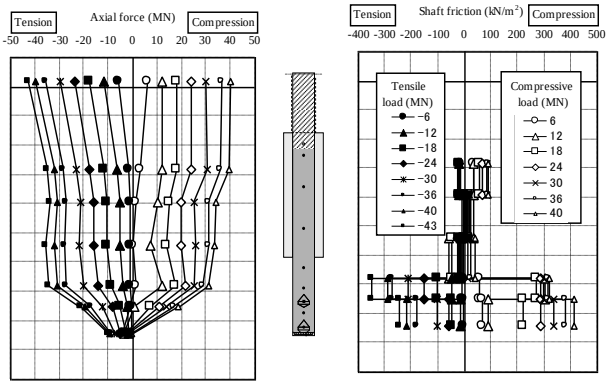

(a) Axial force (b) Shaft friction

Figure 26 Distributions of axial force (left) and shaft friction (right)

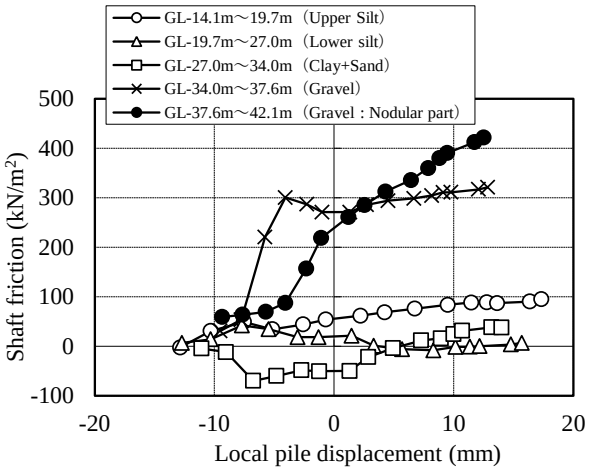

Figure 27 Relationships between shaft friction and displacement in stage of the compression load test

5. EMPIRICAL DESIGN FORMULA OF NODULAR PART AND UNDER-REAMED PART

A number of load tests have been carried out on nodular piles and nodular walls by Obayashi Corporation, in addition to the load tests presented in this paper. In these load tests, axial force measurements were carried out thoroughly in order to estimate the bearing pressure of nodular parts. It may be useful to establish empirical design formula for estimation of the bearing pressure of nodular part based on these test results.

Figure 29 shows the projection areas (bearing areas) of nodular part for nodular pile and nodular wall for calculation of the bearing pressure.

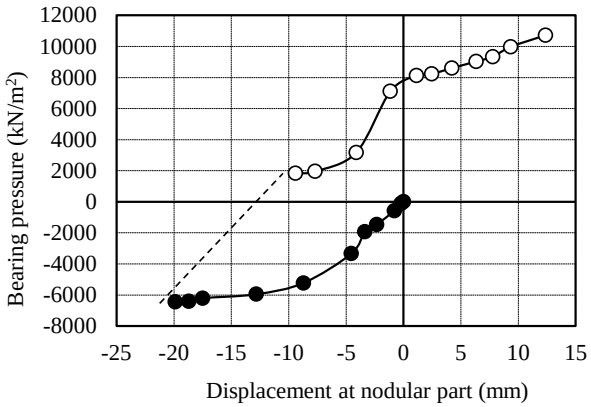

Figure 28 Relationships between bearing pressure and displacement at the nodular part

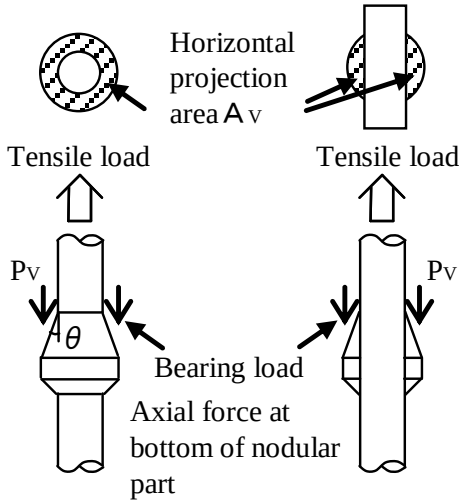

Figure 29 Projection areas of nodular part for nodular pile and nodular wall

The hatched area in Figure 30 shows the assumed influential zone on the bearing pressure of nodular part. It was assumed in establishment of empirical formula that the bearing pressure is governed by soil strength along the influential zone. Influential zones are different for nodular pile and nodular wall and for compression and tension loading.

Equations (1) and (2) are the proposed empirical equations for estimation of pv for sandy and clayey soils, respectively.

$$\text{Sandy soil: } p_v = 100\overline{N}\,(\overline{N} \le 60,\ p_v \le 6000kN/m^2) \quad (1)$$

$$\text{Clayey soil: } p_v = 6c_u\,(c_u \ge 750,\ p_v \le 7000kN/m^2) \quad (2)$$

Where,

p_v: Bearing pressure of nodular part (kN/m^2)
$\overline{N}$: Average SPT N-value along the influential zone
c_u: Average undrained shear strength along the influential zone (kN/m^2)

The length of influential zone, L_N, is given by Eq. (3).

$$L_N = h_N + 3D_N \quad (3)$$

where,

h_N: Height of inclined part (m)
D_N: Width of projecting part (m)

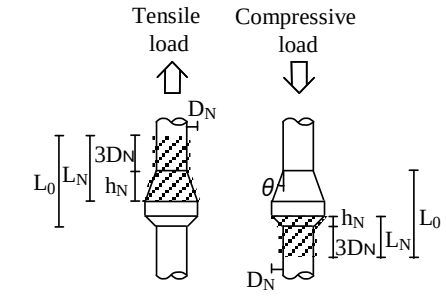

(a) Nodular pile

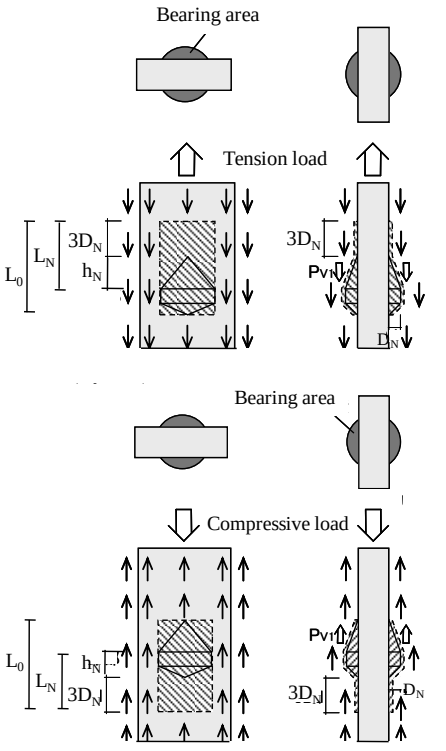

(b) Nodular diaphragm wall

L_N: Calculation range of average N value and undrained shear strength
L_0: Neglecting range of shaft friction

Figure 30 Calculation area of N-value

Figure 31 compares the measured bearing pressures with the calculated values using Eqs. (1) and (2) for nodular piles and nodular walls constructed in various types of soils. It can be seen that the proposed empirical equations give a lower bound of the measured bearing pressures, indicating that the proposed empirical equations can be used for design purpose.

The shaft friction except for the nodular section of length L_0 is calculated by Eqs. (4) and (5) specified in Recommendation for the Design of Building Foundations in Architectural Institute of Japan. (2001).

$$\text{Sandy soil: } \tau = 3.3N(kN/m^2) \quad (4)$$

$$\text{Clayey soil: } \tau = c_u(kN/m^2) \quad (5)$$

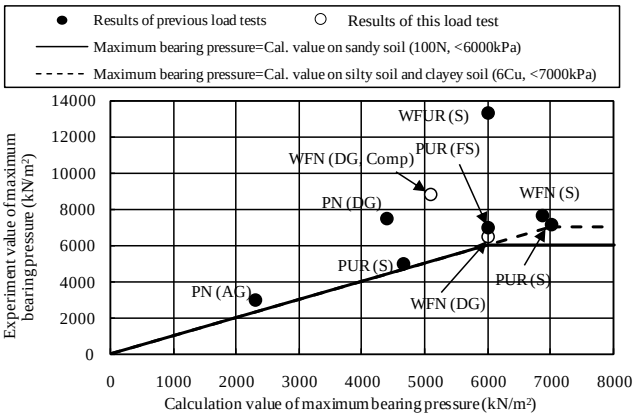

Types of foundations	Types of soils shown in parentheses
WF: Wall foundation	DG: Diluvium gravel
P: Pile	AG: Alluvium gravel
UR: Under-reamed part	S: Silty sand
N: Nodular part	FS: Fine sand
T: Tip part without enlargement	

Figure 31 Relationships between experiment value and calculation value on maximum bearing pressure

6. CONCLUDING REMARKS

The paper described the results on the foundation elements of in-situ full-scale load tests supporting a high-rise tower. The following findings were obtained.

1) The purpose of the first tension load test was to examine the tension resistance at the design wall head. As a result of the first tension load test, it may be concluded that the nodular diaphragm wall has large tension resistance. The tension resistance of nodular diaphragm wall satisfied the design requirement load on the design of wall foundation.
2) The second tension load test with reducing the shaft friction around the test diaphragm wall was carried out to confirm the resistance of nodular part because the tension load couldn't transmit to the nodular part in the first tension load test. It is said that the tension resistance of nodular part indicates a large value.
3) The first and second tension load tests were carried out to obtain the required data for the design of high-rise tower. It is found from these tension load tests that the diaphragm walls have the enough tension resistance to design the foundation of high-rise tower.
4) The nodular diaphragm walls have the enough compression resistance on the design of foundation, because the diaphragm walls were embedded in very hard soil layers. The compression load test with reducing the shaft friction around the test diaphragm wall was carried out as the additional experiment to develop the nodular diaphragm wall and to examine the resistance of nodular part. It is observed that the bearing pressure at the nodular part shows a large resistance.
5) A number of load tests on nodular piles and nodular diaphragm walls have been carried out. Based on the results of these load tests, the empirical design formulas for estimation of the bearing pressure of nodular part are proposed. It is said that these formulas are so useful for design of nodular piles and nodular diaphragm walls.

7. REFERENCES

Architectural Institute of Japan. (2001) "Recommendation for Design of Building Foundations" (in Japanese).

Japanese Geotechnical Society. (2002) "Standards of the Japanese Geotechnical Society (Method for Vertical Load Test of Piles)" (in Japanese).

Keii, M., Konishi, A., Kagami, Y., Watanabe, K., Nakanishi, N. and Esaka, Y (2009) "Structural outline of Tokyo Sky Tree.", Journal of JSSC, JSSC, pp. 12–17 (in Japanese).

Naganuma, K. and Yamaguchi, T. (1990) "Tension Stiffening Model under In-plane Shear Stress.", Proceedings of Annual National Conference on Architectural Institute of Japan, pp. 649-650 (in Japanese).

Naganuma, K. and Ohkubo, M. (2000) "An Analytical Model for Reinforced Concrete Panels under Cyclic Stresses.", Journal of Structural Const. Engineering, Architecture Institute of Japan, No. 536, pp. 579-584 (in Japanese).